This article is a *Plant Cell* Advance Online Publication. The date of its first appearance online is the official date of publication. The article has been edited and the authors have corrected proofs, but minor changes could be made before the final version is published. Posting this version online reduces the time to publication by several weeks.

Arrangement of Photosystem II and ATP Synthase in Chloroplast Membranes of Spinach and Pea [W] [OA]

Bertram Daum,[a] Daniela Nicastro,[b] Jotham Austin II,[c] J. Richard McIntosh,[d] and Werner Kühlbrandt[a,1]

[a] Max Planck Institute of Biophysics, 60438 Frankfurt am Main, Germany
[b] Biology Department, Brandeis University, Waltham, Massachusetts 02453
[c] Advanced Electron Microscopy Facility, University of Chicago, Chicago, Illinois 60637
[d] Department of MCD Biology, University of Colorado, Boulder, Colorado 80301

We used cryoelectron tomography to reveal the arrangements of photosystem II (PSII) and ATP synthase in vitreous sections of intact chloroplasts and plunge-frozen suspensions of isolated thylakoid membranes. We found that stroma and grana thylakoids are connected at the grana margins by staggered lamellar membrane protrusions. The stacking repeat of grana membranes in frozen-hydrated chloroplasts is 15.7 nm, with a 4.5-nm lumenal space and a 3.2-nm distance between the flat stromal surfaces. The chloroplast ATP synthase is confined to minimally curved regions at the grana end membranes and stroma lamellae, where it covers 20% of the surface area. In total, 85% of the ATP synthases are monomers and the remainder form random assemblies of two or more copies. Supercomplexes of PSII and light-harvesting complex II (LHCII) occasionally form ordered arrays in appressed grana thylakoids, whereas this order is lost in destacked membranes. In the ordered arrays, each membrane on either side of the stromal gap contains a two-dimensional crystal of supercomplexes, with the two lattices arranged such that PSII cores, LHCII trimers, and minor LHCs each face a complex of the same kind in the opposite membrane. Grana formation is likely to result from electrostatic interactions between these complexes across the stromal gap.

INTRODUCTION

The site of photosynthesis, by which green plants and algae convert sunlight into chemical energy and evolve oxygen is the thylakoid membrane in the chloroplast interior. The thylakoid membrane segregates laterally into stacked grana disks and nonstacked stroma lamellae (Andersson and Anderson, 1980; Arvidsson and Sundby, 1999; Wehrmeyer, 1964), which contain different sets of membrane protein complexes (Dekker and Boekema, 2005). Three-dimensional (3D) volumes based on serial plastic sections (Mustardy and Garab, 2003) support a widely accepted model (Mustardy et al., 2008) by which stroma thylakoids wind helically around grana stacks, linking individual disks by narrow membrane connections.

Five major membrane protein complexes (the light-harvesting complexes I and II [LHCI and LHCII], photosystems I and II [PSI and PSII], and the cytochrome b_6/f complex) cooperate to generate a proton gradient across the thylakoid membrane by light-driven charge separation (for a review, see Nelson and Ben-Shem, 2004). The atomic structures of most of these complexes have been determined (for reviews, see Jensen et al., 2007; Kern and Renger, 2007; Baniulis et al., 2008; Fromme and Grotjohann, 2008; Renger and Renger, 2008; Schmid, 2008; Barros and Kühlbrandt, 2009), providing detailed insight into the molecular mechanisms of light harvesting and proton and electron transfer. The chloroplast F_1F_o ATP synthase (cF_1F_o) uses the proton gradient to generate ATP. A low-resolution electron microscopy (EM) map of the cF_1F_o complex (Mellwig and Böttcher, 2003) indicates the same basic structure as in the homologous bacterial and mitochondrial enzymes (Stock et al., 1999), consisting of an F_o rotor assembly in the membrane and the catalytic F_1 part that protrudes into the chloroplast stroma.

The distribution of PSII, LHCI and II, cytochrome b/f, and cF_1F_o in plant thylakoids has been investigated for many years. EM of freeze-fractured thylakoids (Staehelin, 1975; Armond et al., 1977; Machold et al., 1977; van Roon et al., 2000; Kirchhoff et al., 2007), plastic sections (Staehelin et al., 1976; Kreuz et al., 1986), and negatively stained membranes (Boekema et al., 2000) have shown that PSII and LHCII account for the bulk of stacked grana thylakoids. PSI, LHCI, and ATP synthase are found in the nonstacked stroma lamellae, whereas cytochrome b/f is thought to be distributed equally throughout both types of lamellae (Dekker and Boekema, 2005). This lateral heterogeneity of the thylakoid membrane has been proposed to maximize the packing density of photosynthetic complexes (Mustardy and Garab, 2003) and to play a role in optimizing light harvesting and energy transfer under changing light conditions. It is also thought to be necessary for state transitions and PSII repair after photoinhibition or nonphotochemical quenching (Anderson et al., 2008). Until now, however, it has not been possible to visualize the in

[1] Address correspondence to werner.kuehlbrandt@biophys.mpg.de.
The authors responsible for distribution of materials integral to the findings presented in this article in accordance with the policy described in the Instructions for Authors (www.plantcell.org) are: Daniela Nicastro (nicastro@brandeis.edu) and Werner Kühlbrandt (werner.kuehlbrandt@biophys.mpg.de).
[W] Online version contains Web-only data.
[OA] Open Access articles can be viewed online without a subscription.
www.plantcell.org/cgi/doi/10.1105/tpc.109.071431

situ arrangement of these complexes in chloroplasts in untreated, unstained membranes.

There is strong evidence that PSII in grana membranes functions as a dimer (Seibert et al., 1987; Peter and Thomber, 1991; Barbato et al., 1992; Santini et al., 1994; Boekema et al., 1995; Hankamer et al., 1997, 1999; Kruse et al., 1997; Morris et al., 1997; Ferreira et al., 2004; Nelson and Ben-Shem, 2004; Nield and Barber, 2006; Watanabe et al., 2009). The PSII dimers are surrounded by up to six LHCII trimers and several minor LHCII molecules in a supramolecular assembly (Dekker and Boekema, 2005; Nield and Barber, 2006). The basic unit of these assemblies is the C_2S_2 supercomplex, which consists of a PSII dimer, two LHCII trimers, and most likely two copies each of the minor LHCs, CP26 and CP29 (Boekema et al., 1998, 1999; Nield and Barber, 2006). The C_2S_2 supercomplex is the most prominent form of PSII in chloroplasts adapted to high light. In low-light conditions, additional LHC trimers and CP24 join to form the larger $C_2S_2M_2L_x$ complex (Boekema et al., 1999; Morosinotto et al., 2006; Betterle et al., 2009). PSII/LHCII supercomplexes can be purified as a sandwich of two dimers, in which the complexes are in close contact with each other through their flat stromal surfaces (Nield et al., 2000). Crystal contacts of LHCII trimers in a two-dimensional (2D) lattice have suggested that LHCII mediates grana formation by electrostatic interactions (Standfuss et al., 2005), but these interactions have not yet been visualized in thylakoid grana. It is thought that PSII and LHCII can rearrange in the grana from a random to a more ordered distribution (Dekker and Boekema, 2005; Kirchhoff et al., 2007). Spectroscopic studies have implied the formation of three-dimensionally ordered arrays of LHCII in chloroplast thylakoids (Barzda et al., 1994), but it has remained unclear whether these arrays are confined to the antenna complexes or contain PSII reaction centers as well. For a full understanding of plant photosynthesis, it is necessary to establish how the PSII supercomplexes are organized and interact with one another in the thylakoid membrane.

The structure of the chloroplast ATP synthase (cF_1F_o) has been determined to a resolution of 20 Å by single-particle EM (Mellwig and Böttcher, 2003). For steric reasons, the complex is found only in the nonstacked regions of the thylakoid membrane (Oleszko and Moudrianakis, 1974; Miller and Staehelin, 1976), since the bulky F_1 subunit is too large to fit in the stromal gap between stacked grana thylakoids (Staehelin et al., 1976). In mitochondria, rows of dimeric ATP synthases are associated with the most highly curved regions of tubular or lamellar inner membrane cristae (Strauss et al., 2008). The dimers of the mitochondrial ATP synthase are thought to induce a high local membrane curvature that enables protons pumped through the membrane by respiratory chain complexes to be collected and used effectively for ATP production in mitochondria (Strauss et al., 2008). Recent data obtained by blue-native gel electrophoresis of solubilized thylakoid membranes suggest that cF_1F_o in *Chlamydomonas reinhardtii* may likewise form dimers (Rexroth et al., 2004). Electron micrographs of negatively stained thylakoid membranes (Dekker and Boekema, 2005) have also implied a dimer-like arrangement of ATP synthase in higher plants.

Here, we report the direct observation of PSII dimers and ATP synthase within chloroplast thylakoids of higher plants by electron cryotomography of intact chloroplasts in vitreous sections and of plunge-frozen suspensions of isolated thylakoid membranes. The technique is capable of visualizing the 3D organization of protein complexes in their membrane environment with ~4- to 5-nm resolution (Leis et al., 2009). We observed that PSII/LHCII complexes are more highly ordered and more tightly packed in stacked than in nonstacked membranes; occasionally, they form crystalline arrays. Thylakoid membranes in grana stacks interact across the stromal gap in a locally ordered manner. We also show that the ATP synthases in plant thylakoids are monomers located on minimally curved stromal thylakoids or grana end membranes, but they are absent from the highly curved grana margins, in clear contrast with the situation in mitochondria.

RESULTS

Grana and Stroma Thylakoids

Suspensions of intact, light-treated chloroplasts from fully developed spinach (*Spinacia oleracea*) leaves were high-pressure frozen, and vitreous sections were cut for tomographic tilt series. Grana stacks sectioned in a direction perpendicular to the membrane plane were evident as straight, dark, parallel lines with average lengths of 350 to 550 nm, separated by less dense lumenal and stromal spaces (Figure 1A). Lumen and stroma were easily distinguished at the edge of the grana because the space between stacked thylakoids is continuous with the chloroplast stroma, whereas the lumenal space is enclosed by the thylakoid membrane. The stromal space was noticeably darker than the lumenal space, suggesting a higher protein content. For a reliable and accurate measurement of the stacking repeat, we calculated the power spectrum (see Methods; Figure 1C) of a cross-sectioned grana stack (Figure 1B). This indicated a repeat distance of 15.7 nm, which corresponds to the height of a grana disk plus the stromal gap.

The number of thylakoids within a grana stack ranged from 5 to 20. In some regions, the connections between stacked grana and unstacked stroma thylakoids were clearly visible at the grana margins (Figure 1D). In single slices through the tomogram, the stroma lamellae were either continuous with a grana disk (Figure 1D; green arrowheads) or they bifurcated, connecting two adjacent grana thylakoids within a stack (Figure 1D; blue arrowheads). When examining the 3D volume, it was clear that at the grana-stroma interface one stroma lamella divided into two or more short lamellar protrusions, which connected successive grana thylakoids in a stepwise manner (Figures 1E to 1G). The plane of a stroma thylakoid was tilted by ~10 to 15° relative to the plane of the grana disks, with the direction of the tilt following the sequence of the connections. Each grana disk can be connected to more than one stroma lamella.

We also attempted to examine entire pea (*Pisum sativum*) chloroplasts by electron tomography of a plunge-frozen suspension. Whole chloroplasts were too thick for electron tomography, but occasionally, they had ruptured during blotting due to surface tension. In these ruptured chloroplasts, we were able to

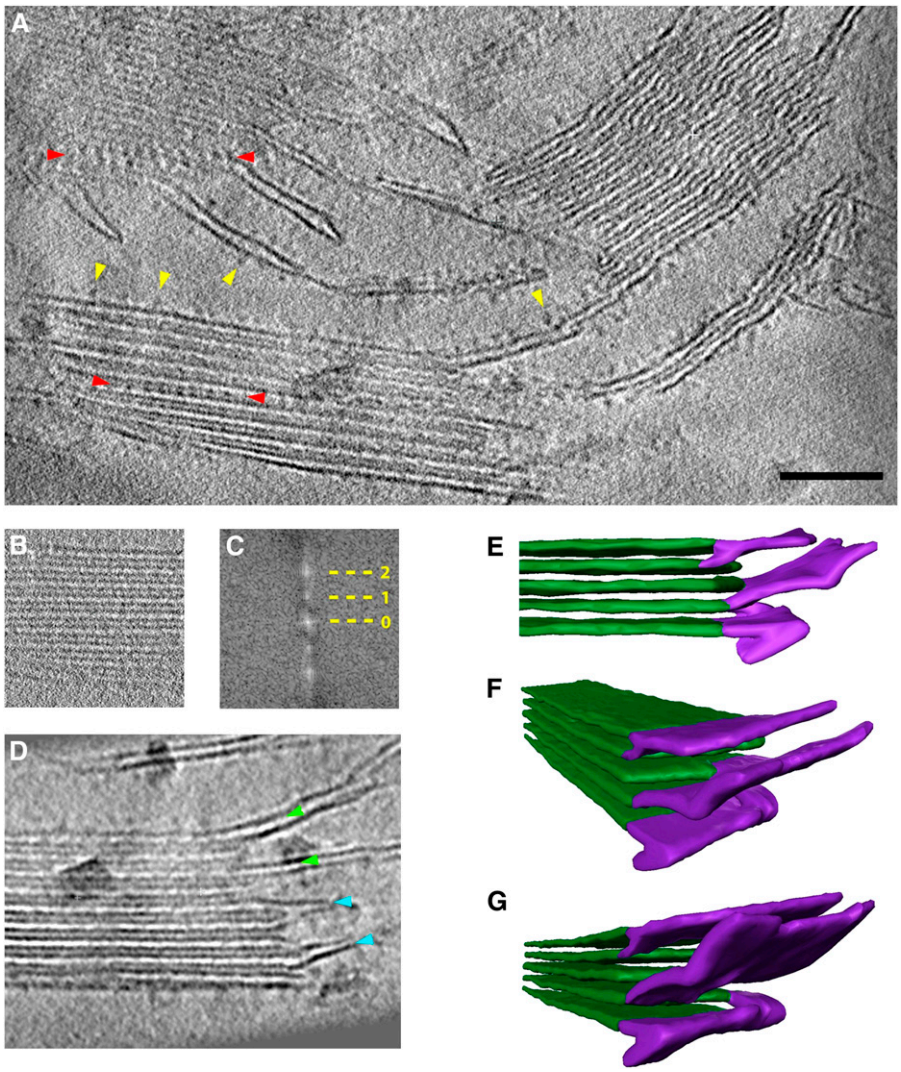

Figure 1. Electron Tomography of Vitreous Spinach Chloroplast Sections.

(A) Tomographic slice through the 3D reconstruction of a vitreous chloroplast section. Stacked grana and unstacked stroma thylakoid membranes are easily distinguished. ATP synthase molecules (yellow arrowheads) protrude from the flat regions of grana end membranes and unstacked stromal thylakoids into the stroma. Rows of PSII complexes with a regular repeat distance are visible within some grana membranes (red arrowheads). Bar = 100 nm.

(B) and **(C)** The accurate stacking repeat of grana thylakoids in a subvolume **(B)** is shown by its power spectrum **(C)**. Zero, first, and second orders indicate a repeat distance of 15.7 nm.

(D) Stroma thylakoids either are continuous with a grana thylakoid (green arrowheads) or bifurcate to merge with two adjacent grana thylakoids (blue arrowheads).

(E) to **(G)** Surface representation of connections between grana (green) and stroma (purple) thylakoids reveals their 3D organization at the grana margin. The stroma lamellae are often tilted with respect to the plane of the grana membranes.

(E) Subvolume of a grana stack with two stroma thylakoids.

(F) and **(G)** Two different views of the grana stack shown in **(E)**. For simplicity, each thylakoid is depicted as a solid volume rather than a membrane pair.

view minimally disturbed, entire thylakoid networks of stacked grana disks and unstacked stromal membranes, as shown in the Supplemental Movie online. We observed two circular, disk-like grana stacks containing numerous PSII dimers in six or eight subsequent membrane layers, while the grana end membranes and stromal membranes were studded with cF_1F_o ATP synthase. Apart from these two large, easily distinguishable membrane protein complexes, we also visualized large numbers of other, as yet unidentified membrane proteins, as well as several dense, apparently membrane-associated particles that we interpret as chloroplast ribosomes and small spherical structures that we believe to be plastoglobules.

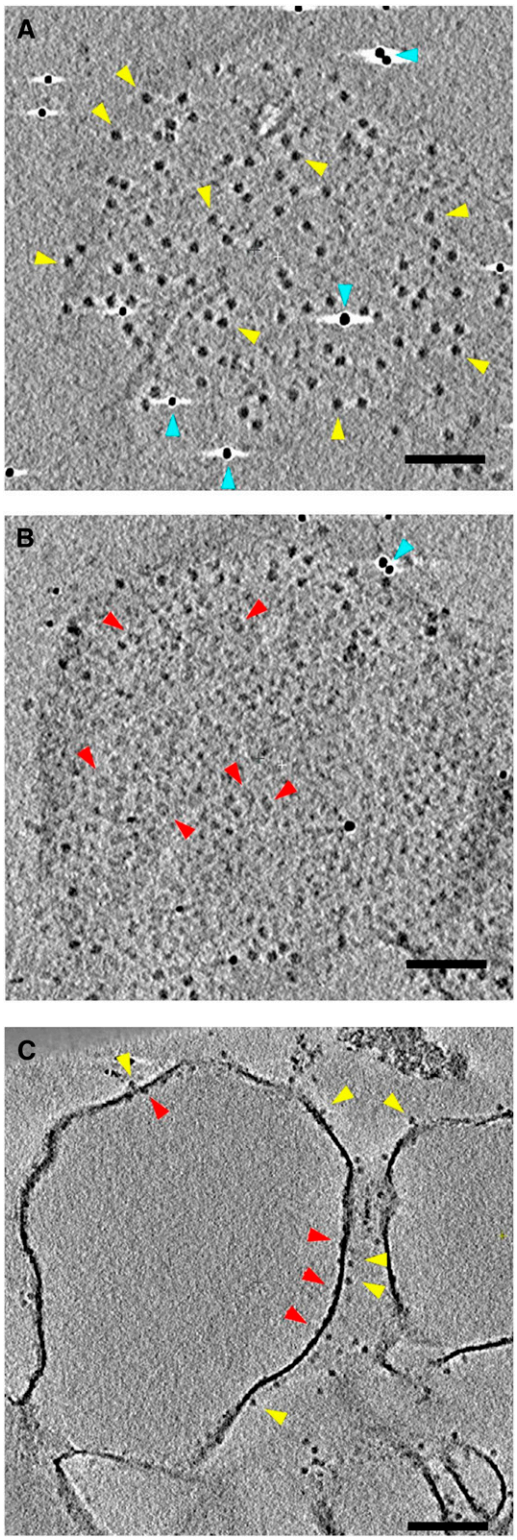

Figure 2. Electron Tomography of Plunge-Frozen, Isolated Thylakoid Membranes.

Three tomographic slices at different z heights and angles through the same tomogram of a plunge-frozen, unstacked pea thylakoid membrane prepared by osmotic shock. The tangential slices in **(A)** and **(B)** run parallel to the thylakoid membrane, ~9 nm above **(A)** or ~3 nm below **(B)** the membrane surface. In the slice along the stromal side of the membrane **(A)**, the cF_1 heads of the ATP synthase are seen as dark, uniform 12-nm globular protein densities (yellow arrowheads); several dense ~6-nm gold fiducial markers, used for tomographic reconstruction of the tilt series, are also seen (blue arrowheads, white shadows). The slice in **(B)** on the lumenal side of the membrane shows dimers of the OEC (red arrowheads) as well as numerous smaller protein densities that cannot be assigned. The tomographic slice in **(C)** cuts at right angles through the thylakoid membrane, so that the OECs (red arrowheads) and ATP synthase (yellow arrowheads) are seen on opposite sides of the membrane. Bars = 100 nm.

In Situ Arrangement of PSII

Tomograms of stacked grana thylakoids in vitreous sections (Figure 1A) as well as tomograms of isolated thylakoids (Figures 2 and 3) or of entire chloroplasts ruptured on the EM grid (see Supplemental Movie online) showed clear densities within the membrane that protruded ~4.5 nm into the thylakoid lumen (Figures 3B, 3G, and 3I). In side views, these protrusions were most evident where two grana thylakoids were in contact across the stromal gap (Figures 1A, 3G, and 3I). When viewed in a direction perpendicular to the membrane plane, the particles were roughly rectangular in outline and clearly dimeric (Figures 2B, 3A, and 3H). The position, dimensions, and arrangement of these densities indicated that they were dimeric reaction center complexes of PSII. By far the most of the clearly distinguishable particles in stacked grana membranes were PSII dimers. Smaller, differently shaped particles, possibly monomeric PSII or cytochrome b_6/f complexes, were also observed, but could not be assigned to either with confidence.

More than 300 PSII dimers were aligned and averaged using Particle Estimation for Electron Tomography software (Nicastro et al., 2006) to show their structure more clearly (Figures 3C and 3E). The PSII dimers contained two roughly kidney-shaped densities, each measuring 8.9 nm in length and 2.5 nm in width, related by a twofold symmetry axis perpendicular to the membrane. Comparison with EM maps of PSII/LHCII supercomplexes (Nield and Barber, 2006) rendered to 3-nm resolution (Figures 3D and 3F) indicates that the protruding densities belong to the oxygen-evolving complex (OEC).

In vitreous sections, as well as in isolated thylakoids, the OECs were closely packed in appressed thylakoid membranes (Figure 1A) and in thylakoid vesicles that contained both appressed and nonappressed membranes (Figures 3G and 3I). The particles appeared to be arranged in rows when viewed in cross sections through the appressed thylakoids (Figures 3G and 3I), whereas the nonappressed membranes, which are, in effect, grana end membranes, contain ATP synthases (Figure 3I), as expected. The particle rows were not visible in unstacked thylakoids (Figures 2B and 2C). In several regions, the complexes in adjacent membranes were separated by a regular center-to-center spacing of ~18.5 nm across the stromal gap (Figure 3I). In these regions, the particles in one membrane were in register with those in the opposite membrane, suggesting a specific interaction across the

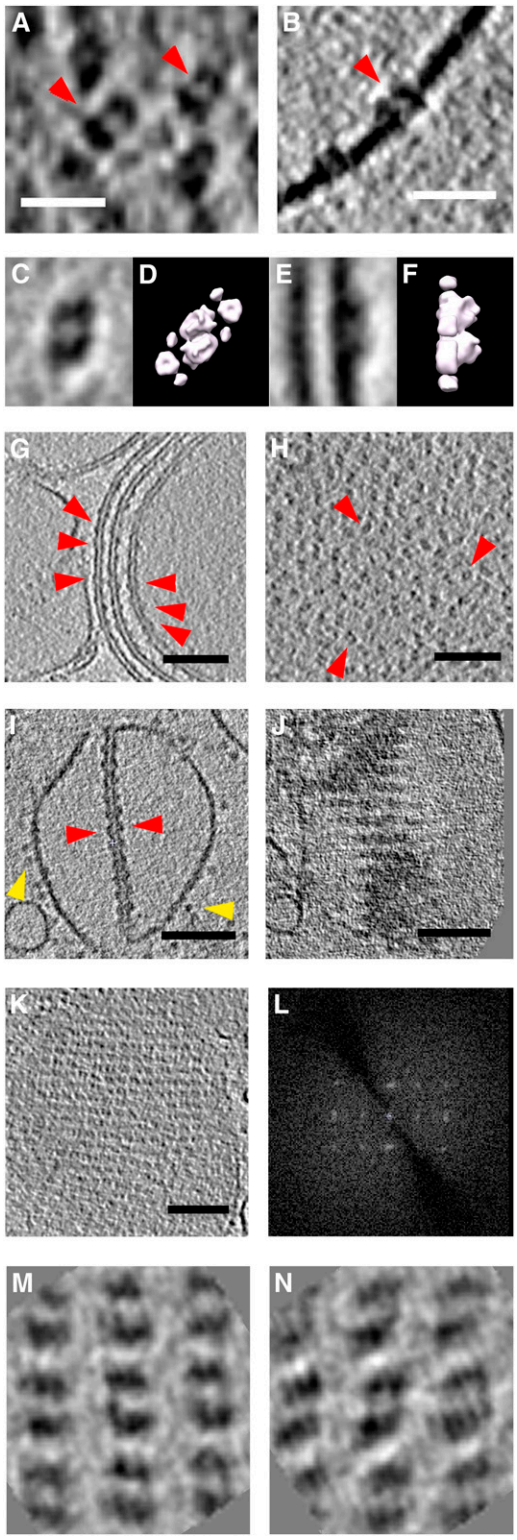

Figure 3. Organization of PSII in Grana Thylakoids.

Detailed views of tomograms from isolated thylakoid membranes. Membranes isolated from pea chloroplasts by osmotic shock (**[A]** and **[B]**) or from spinach by mild digitonin treatment (**[C]**, **[E]**, and **[G]** to **[N]**).

stromal gap. When viewed in slices parallel to the membrane plane, the PSII complexes in these rows were seen to form regular, 2D crystalline arrays (Figures 3J to 3N).

Mild detergent treatment or hypo-osmotic shock of isolated thylakoids frequently resulted in swollen vesicles in which the interaction of OECs was lost across the lumenal space, but the stromal surfaces of grana thylakoids remained tightly appressed (Figures 3G and 3I). The intact interaction across the stromal gap was suggested by its constant size and the rows of OECs (Figure 3I). Regular 2D arrays of PSII particles were also observed in swollen thylakoids that remained stacked (Figures 3I and 3J). While swollen thylakoids usually had irregular, curved shapes, the surfaces that contained crystalline PSII arrays were almost perfectly flat.

The PSII arrays in each membrane had in-plane twofold (*p*2) symmetry with lattice dimensions a = 19.5 nm, b = 17.7 nm, including an angle of ~90° (see power spectrum in Figure 3L). The C_2S_2 PSII supercomplex fitted into this lattice perfectly, whereas a supercomplex with additional antenna proteins was too large. To analyze the protein interactions within appressed crystalline arrays, the 3D map of the C_2S_2 PSII/LHCII supercomplex (Nield and Barber, 2006) was fitted manually to the volume of the averaged PSII densities (Figures 3M and 3N), using the protruding OECs for alignment. The resulting arrangement of PSII/LHCII supercomplexes is shown in Figure 4A. Within one such model membrane, supercomplexes are arranged head-to-tail, forming diagonal rows that include an angle of ~50° with the horizontal axis. The rows are separated by an ~2-nm gap that is most likely filled with lipid. The closest contacts between supercomplexes within one layer are between the peripheral densities that have been ascribed to minor LHCs (Nield and Barber, 2006). The lattice in the other, appressed membrane is related to the first layer by a 180° rotation about an axis along either of the crystal axes, at a position half way between the two membranes. The entire crystalline array including both membranes thus has *p*222 symmetry.

(A) OECs (red arrowheads) protruding from the membrane surface in a tomographic slice parallel to the membrane.
(B) Cross section of PSII dimers with OECs (red arrowhead) in the thylakoid membrane. Bars = 20 nm in **(A)** and **(B)**.
(C) to **(L)** Top **(C)** and side view **(E)** of averaged OEC volumes, compared with the top **(D)** and side view **(F)** of the PSII/LHCII supercomplex (Nield and Barber, 2006) drawn at 3-nm resolution. PSII complexes (red arrowheads) are closely but randomly packed in destacked grana thylakoids, as seen in cross **(G)** and tangential sections **(H)** of tomographic volumes. In stacked grana thylakoids, PSII complexes occasionally form pairs of crystalline arrays, as seen in cross **(I)** or oblique sections **(J)** of a pair of thylakoid vesicles that contain both stacked and unstacked membranes. Yellow arrowheads point to ATP synthases in the unstacked membrane regions that are, in effect, grana end membranes. A tomographic slice of such a PSII array cut parallel to the membrane plane **(K)** and its power spectrum **(L)** clearly shows the crystallinity. Bars = 100 nm in **(G)** to **(K)**.
(M) and **(N)** Slices through each of the two crystalline PSII arrays indicate that the two lattices of the membrane pair are in register across the stromal gap, forming together a 2D crystal of *p*222 symmetry.

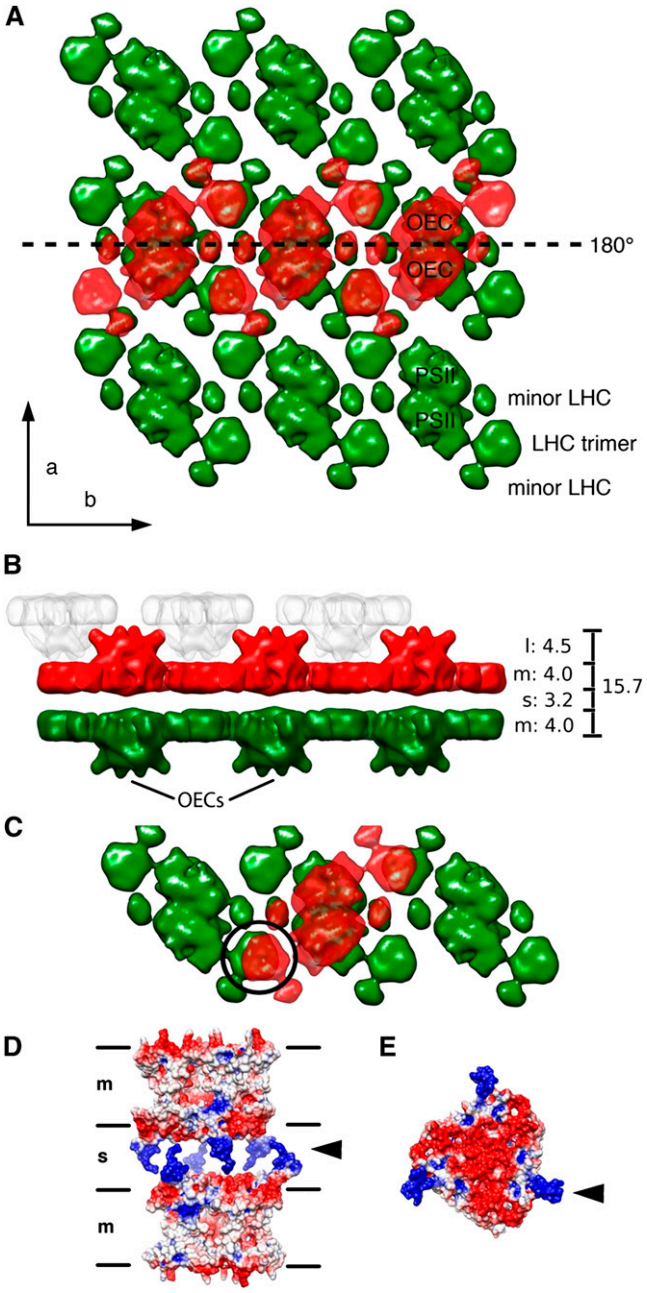

Figure 4. Interaction of PSII/LHCII Supercomplexes in Appressed Grana Thylakoids.

(A) A 3D map of the PSII/LHCII supercomplex (Nield and Barber, 2006) at 3-nm resolution fitted manually to the averaged 2D lattices shown in Figures 3M and 3N, respectively. The lower layer is shown in green and the upper layer in red. The OECs in the upper layer face the viewer. The two layers are related by an in-plane twofold axis (dashed line). The flat stromal surfaces of the supercomplexes are in contact across the stromal gap, while the OECs project into the lumenal space. In this arrangement, the PSII dimers, LHCII trimers, and minor LHCs each interact with another complex of the same kind in the opposite membrane. Black arrows indicate the crystal axes *a* and *b* of the 2D array.
(B) Side view of **(A)**. The bar on the right indicates how the lumenal gap (l), the two membranes (m), and the stromal gap (s) add up to the stacking repeat distance of 15.7 nm (all distances in nm). The narrow lumenal gap means that the OECs of PSII complexes in one grana thylakoid (red and gray) interdigitate.
(C) View of four supercomplexes as in **(A)**, showing how a single supercomplex (red) connects to three others (green) in the opposite membrane.
(D) Electrostatic surfaces calculated from the x-ray structure (Standfuss et al., 2005) of two LHCII trimers at pH 8.0 in the arrangement entailed by the interacting PSII arrays (black circle in **[C]**). In this arrangement, the modeled, positively charged N termini (blue) interact with the negatively charged stromal surface (red) of the opposite trimer. Black lines delineate the membranes (m) and the stromal gap (s).
(E) Charge distribution on the stromal surface of one LHCII trimer. Black arrowheads in **(D)** and **(E)** indicate the positively charged N termini.

Contacts between PSII/LHCII supercomplexes in both membranes are mediated in our model by the stromal surfaces of both the LHCs and the PSII reaction center dimers. Note that in this arrangement, the LHCII trimers at either end of one supercomplex sit on top of the LHCII trimers in the opposite membrane, such that each supercomplex in one membrane spans three rows of supercomplexes in the other (Figure 4C). Moreover, the smaller densities that have been assigned to minor LHCs (Nield and Barber, 2006) are each on top of another density of the same kind in the opposite membrane. In this way, each supercomplex in one membrane interacts with up to five supercomplexes in the other layer. When the assembly is viewed from the side (Figure 4B), it closely resembles the rows of densities seen in Figures 1A and 3I.

Visual inspection of Figure 1B indicated that the total thickness of a grana disk was 8.5 nm, measured as the center-to-center distance between the two membranes of one disk. The center-to-center distance between appressed membranes across the stromal gap was 7.2 nm. These two dimensions added up to the grana thylakoid repeat distance of 15.7 nm. Allowing for an approximate membrane thickness of 4 nm, the average widths of the lumenal and stromal spaces were thus 4.5 and 3.2 nm, respectively (Figure 4B). The stromal gap accommodates the N-terminal peptides of LHCII (Figures 4D and 4E), which contain several Arg and Lys residues. These positively charged regions of the LHCII polypeptide were not resolved in the x-ray structure (Standfuss et al., 2005), indicating that they are disordered and hence able to interact flexibly with the negatively charged stromal surface of the opposite LHCII trimer. In the arrangement entailed by our crystalline membrane model (Figures 4A and 4B), the N-terminal peptides of two adjacent LHCII trimers happen to interdigitate, as shown in Figure 4D, consistent with the well-documented strong electrostatic interaction between appressed grana thylakoids (Barber, 1982; Staehelin, 1986). Most likely, LHCII trimers mediate similar electrostatic interactions between PSII supercomplexes also in the more common, noncrystalline grana thylakoids.

Distribution and Oligomeric State of the Chloroplast ATP Synthase

Numerous protein densities of ~12 nm diameter protruding from the outer surface of grana end membranes and from stromal

thylakoids were observed in vitreous sections of intact spinach chloroplasts (Figures 1A and 5A) and in tomograms of entire pea chloroplasts ruptured on the EM grid (see Supplemental Movie online). These particles extended to ~16 nm above the membrane and usually appeared to be connected to the membrane by an ~4-nm-long, narrow stalk (Figures 5B to 5D). In single and averaged tomographic volumes (Figure 5B to 5E), the shape and dimensions of these particles resembled closely the 3D map of the chloroplast ATP synthase (Mellwig and Böttcher, 2003). As no other membrane protein complex in chloroplast thylakoid membranes has similar features and is expected to occur so frequently, the globular densities are clearly the cF_1 heads of the chloroplast ATP synthase. The cF_1 heads were seen in considerable detail in tomograms of isolated, plunge-frozen pea and spinach membranes (Figures 5B and 5C). Occasionally, the cF_o rotor domain in the membrane was also visible (Figure 5B).

In vitreous sections, the ATP synthase appeared to be more or less evenly distributed over grana end membranes and nonstacked stroma thylakoids, but it was not seen in the tightly appressed grana membranes or in the grana margins (Figures 1A and 5A). The ATP synthase was thus confined to nonappressed, flat, or slightly curved areas but was absent from highly curved membrane regions. All ATP synthase molecules were oriented with their long axis perpendicular to the membrane.

The average distribution of ATP synthase molecules was ~1770 per μm^2, as determined by counting the number of particles in a given membrane area in the tomogram of a vitreous section. The F_1 subunit of the chloroplast ATP synthase has a diameter of 12 nm (Böttcher and Graber, 2000), which corresponds to a surface of 113 nm^2 per molecule or 0.2 μm^2 for 1770 particles. This means that the ATP synthase covers ~20% of the unstacked thylakoid surface, with an average center-to-center distance of 27 nm, or 15 nm edge-to-edge.

Roughly 85% of the ATP synthases were monomeric rather than associated with another similar particle, while 15% appeared to be in contact with a neighboring ATP synthase. Of these, 12% formed pairs, 3% groups of three, and <1% were in groups of four to six monomers (Figure 5E). No larger aggregates or linear assemblies were found. The relative numbers of monomers and small groups were similar in tomograms of vitreous sections and of isolated spinach or pea thylakoid membranes, indicating that the membrane organization in isolated thylakoids had remained largely intact and is not species dependent. Groups of two or more monomers did not have a recognizable, recurring shape (Figure 5E), so the assemblies appeared to be random.

The oligomeric state of cF_1F_o in chloroplast thylakoids was further investigated by native gel electrophoresis of digitonin-solubilized membranes. ATP synthase monomers were identified by an in-gel activity assay (Figures 5F and 5G). A denaturing gel run in the second dimension revealed the typical band pattern (Neff and Dencher, 1999) of cF_1F_o in the clear-native gel bands (Figure 5H). No oligomers were detected under any detergent conditions used, ranging from 0.5 to 3% (w/v).

In fully destacked, isolated thylakoids, ATP synthase and PSII dimers were intermixed (Figures 2A to 2C). The PSII dimers were disordered, less densely packed than in stacked membranes, and interspersed with PSII monomers or smaller complexes (Figure 2B). In cross-sectional views, the OECs of PSII dimers on the lumenal surface and the ATP synthase cF_1 heads on the stromal surface were easily discernible (Figures 2A to 2C). An analysis of particle positions did not reveal any specific interaction between the ATP synthase and PSII in these membranes (data not shown).

DISCUSSION

We have performed electron cryotomography on vitreous sections of spinach chloroplasts and on plunge-frozen pea or spinach thylakoids to study the 3D supramolecular organization of the photosynthetic complexes within the thylakoid membrane. Unlike mitochondria, which can be small enough to allow cryotomography of plunge-frozen suspensions (Frey and Mannella, 2000; Nicastro et al., 2000; Mannella, 2001), whole chloroplasts are too large for this approach. To observe the macromolecular complexes in or at the membrane, it was therefore necessary to cut thin, vitreous sections. As alternative approaches, we examined chloroplasts fortuitously ruptured directly on the EM grid (see Supplemental Movie online) or plunge-frozen preparations of isolated thylakoid membranes. In vitreous sections, the membrane organization of chloroplast thylakoids is unperturbed. Thylakoid networks of ruptured chloroplasts are minimally disturbed, whereas the membrane organization might conceivably change in isolated thylakoids. Tomograms of plunge-frozen, isolated membranes have the advantage of providing better contrast and resolution than vitreous sections. Moreover, vitreous sections suffer from distortions and mechanical damage, such as compression and crevasses (Al-Amoudi et al., 2005), and rarely allow molecular detail to be observed. We therefore decided to combine the advantages these different approaches, examining tomograms of vitreous sections or ruptured chloroplasts to gain insight into the overall organization of the complexes in chloroplasts and isolated, plunge-frozen thylakoids to study the complexes in their membrane environment in greater detail.

Detergents have frequently been used to study the organization of thylakoid membranes and the photosynthetic complexes within them. Thylakoid membranes isolated by the mild detergent treatment employed by us are active in photosynthetic oxygen evolution and protein synthesis (Dunahay et al., 1984), indicating that the membrane organization is intact. However, because detergent might insert into the membrane, we also examined chloroplasts ruptured directly on the EM grid and membranes isolated after osmotic shock, neither of which had been exposed to detergent, to ensure that the detergent treatment did not perturb the protein organization in the membranes.

Although membrane isolation can result in swollen thylakoids, stroma membranes and grana stacks were preserved in our preparations. We found that the overall 3D organization of PSII and ATP synthases was unchanged when compared with vitreous sections of native chloroplasts that had not been subjected to either detergent treatment or osmotic shock. This demonstrates clearly that the swelling of thylakiod vesicles does not affect the organization of the photosynthetic complexes within the membrane. We examined both spinach and pea thylakoids,

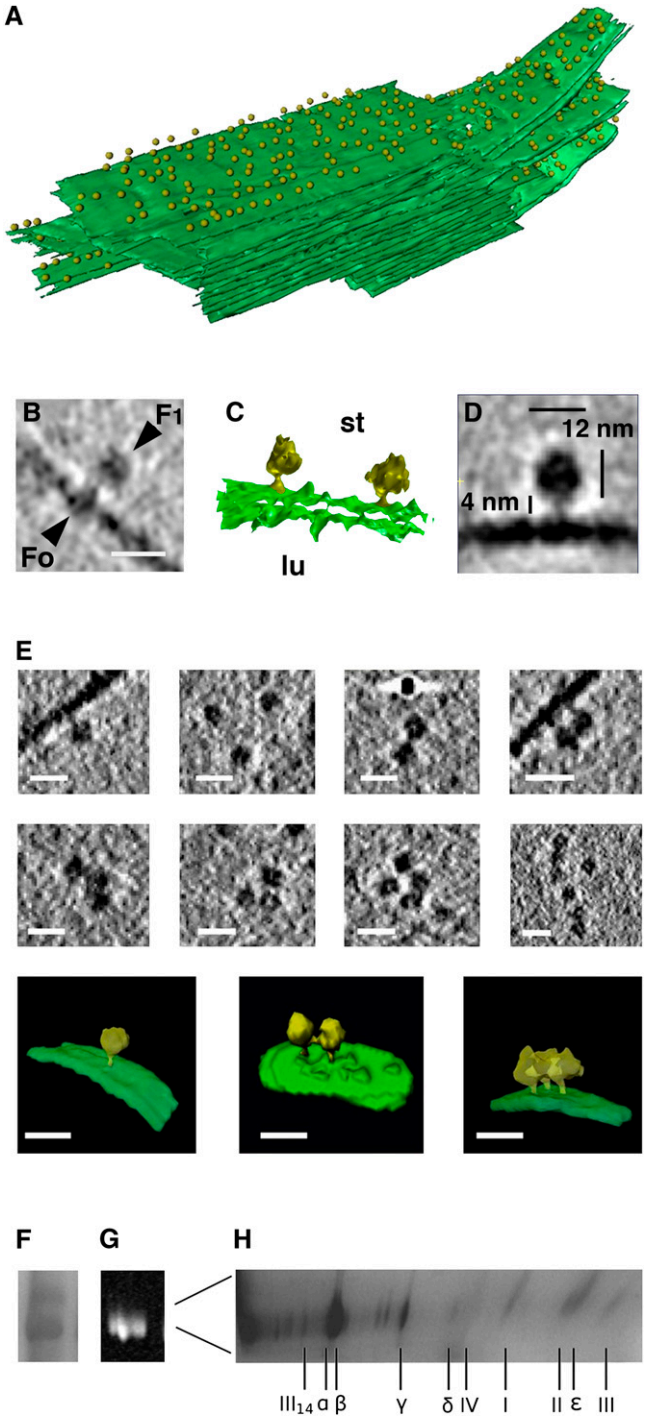

Figure 5. Organization of the Chloroplast ATP Synthase in Thylakoid Membranes.

(A) Segmented subvolume of a grana stack with connected stroma lamellae (green) from a vitreous spinach chloroplast section. Individual ATP synthase molecules are indicated by yellow 12-nm spheres. The ATP synthases are randomly distributed over the minimally curved grana end membranes and stromal lamellae but are absent from the appressed regions within the grana and from the highly curved grana margins.

as these have been used most often in previous studies. As expected, results for both species were interchangeable. Vitreous sections, thylakoid networks of ruptured chloroplasts, and thylakoid membranes isolated with or without detergent all showed the same lateral segregation of PSII complexes in grana stacks and ATP synthase in stromal or grana end membranes.

Stroma and Grana Membranes

Stroma and grana membranes, which contain different sets of protein complexes, merge at the grana margins. This special region of the chloroplast thylakoid system has been examined in several previous studies by serial sections of chemically fixed plant tissue (Mustardy and Garab, 2003) and by tomography of high-pressure frozen, freeze-substituted, and plastic-embedded material (Shimoni et al., 2005; Austin et al., 2006). Our observations were broadly consistent with previous work (Mustardy and Garab, 2003), but we found that the connections between grana and stroma thylakoids were lamellar (Figures 1F and 1G) and appeared to be several times wider than the narrow membrane connections described earlier on the basis of serial plastic sections (Mustardy et al., 2008). The angle between the planes of stroma and grana lamellae was shallower, being 10 to 15° rather than 20° (Mustardy et al., 2008). In the vitreous sections, we observed up to two consecutive grana membranes fused to one stromal lamella, but it is likely that each stroma thylakoid connects more than two grana disks in a stack.

From power spectra of the one-dimensional lattice defined by the stacking repeat of cross-sectioned grana (Figures 1B and 1C), we determined the vertical distance between pairs of membranes in spinach grana as 15.7 nm. Previously reported repeat distances for spinach ranged from 14.4 nm (Murakami and Packer, 1970) to 24.3 nm (Tokuyasu, 1976). It has been proposed that the vertical dimension of grana stacks varies according to light conditions, as they appear to become compressed in high light and expand in the dark (Albertsson, 1982; Anderson et al., 2008). If this is the case, the vertical repeat

(B) Subvolume of a single ATP synthase within an isolated, plunge-frozen pea thylakoid. The cF_1 part, the central stalk, and the cF_o part in the membrane can be distinguished. Bar = 15 nm.

(C) Isosurface representation of two ATP synthase molecules (yellow) in an isolated pea thylakoid membrane (green). lu, lumenal side; st, stromal side.

(D) Single-particle average of 50 ATP synthase volumes obtained from isolated spinach thylakoids. Shape and dimensions are consistent with the chloroplast ATP synthase (Mellwig and Böttcher, 2003).

(E) Gallery of tomographic slices (top two rows) and surface renderings of segmented subvolumes (bottom row) of multiple copies of ATP synthase in isolated pea thylakoid membranes. Most are monomers, some are pairs, and a small number forms random groups of three to six complexes. Bars = 20 nm.

(F) and **(G)** Clear-native PAGE **(F)** and in-gel ATPase assay **(G)** of digitonin-solubilized thylakoid membranes. No ATP synthase oligomers are detected.

(H) Second dimension SDS-PAGE of the active band in **(G)** reveals all subunits of the chloroplast ATP synthase.

distance in our sections is consistent with chloroplasts in a light-adapted state.

The lumenal OECs of the PSII/LHCII supercomplexes in grana stacks have been assumed either to be arranged head-to-head (Anderson et al., 2008) or to interdigitate (Kirchhoff et al., 2008). Since PSII dimers measure ~10.5 nm in the direction perpendicular to the membrane (Anderson et al., 2008), a head-to-head arrangement would thus entail a vertical repeat distance of 24.2 nm (i.e., 21 nm plus the width of the stromal gap, which we determined as 3.2 nm) (Figure 4B). Our observed repeat distance of 15.7 nm precludes such a head-to-head arrangement. Since the width of the lumenal gap corresponds to the height of about one OEC complex above the membrane, the OECs in our tomograms must interdigitate (gray densities in Figure 4B). It would be interesting to see if the arrangements of the PSII supercomplexes changes in different light conditions and whether this might be the reason for the proposed vertical expansion of grana stacks in the dark-adapted state.

The width of the stromal gap determined by us is consistent with previous measurements of conventional thin sections of plastic-embedded chloroplasts, which suggested gap widths ranging from 2 nm (Dekker and Boekema, 2005) to 4 nm (Nir and Pease, 1973). Recent atomic force microscopy studies of detergent-extracted and partially dehydrated thylakoid membranes indicated a stromal gap of ~2.6 nm (Kirchhoff et al., 2008). This suggests that the values at the lower end of this range may be due to dehydration-dependent shrinkage and that our tomograms show the actual 3.2-nm gap distance in high-light thylakoids. The total height of PSII of ~10.5 nm includes the lumenal OEC protrusions (4.5 nm), the membrane-embedded region (4 nm), and some stromally exposed loops projecting up to 2 nm into the stromal gap (Anderson et al., 2008). Thus, a stromal gap of 3.2 nm can easily accommodate the stromal loops of two opposed PSII supercomplexes, considering the rotational offset of PSII complexes in the appressed membranes. Taken together, our observations suggest that membrane appression in grana stacks is at its spatial limits, at least in light-adapted chloroplasts, resulting in a closely interlinked, tightly packed PSII antenna.

PSII Arrays and Grana Stacking

Regular arrays of large particles in chloroplast thylakoid membranes have been reported in the early literature (see Park, 1965; Miller et al., 1976; Simpson, 1983). Most of these regular arrays had unit cell dimensions similar to those reported here. It had been assumed for a long time that the particles are PSII reaction centers (for a review, see Kühlbrandt, 1987), but it was not known which, if any, other chlorophyll-protein complexes were present in the arrays. Considering the close fit of the EM map (Nield and Barber, 2006) to the regular arrays in the tomographic volumes, there can be little doubt that they consist of PSII supercomplexes and thus contain LHCII and most likely minor LHCs, in addition to PSII reaction centers.

The PSII/LHCII supercomplex contains ~130 chlorophyll molecules, while there are up to 250 chlorophylls per PSII reaction center in normal high-light thylakoids (Jansson et al., 1997). This means that each PSII reaction center is, on average, associated with more than one LHCII trimer, so that that the regular arrays cannot account for the entire grana membrane. Indeed, the tomographic volumes show that the grana membranes are not entirely crystalline but that the regular PSII arrays occur as local patches. However, we found that these patches were not infrequent in normal, light-adapted spinach chloroplasts. It follows that they are present under normal physiological conditions and not only in cold-acclimatized plants (Garber and Steponkus, 1976) or LHC mutants (Simpson, 1983), as had been previously suggested. The stromal surfaces of PSII/LHCII supercomplexes can evidently interact in other geometries, for example, in the supercomplex sandwich dimers examined by single-particle EM (Nield et al., 2000). Note, however, that also in these sandwich dimers, the LHCII trimers would interact similarly as in the 2D arrays. It is therefore safe to conclude that the transmembrane interactions that govern grana stacking in native chloroplasts are very similar to those that hold the PSII arrays together and that the electrostatic interactions between LHCII trimers and minor LHCs are a key factor in stacking. Thus, the interactions of PSII/LHCII supercomplexes visualized in this study play a key role in establishing the striking lateral heterogeneity between stroma and grana membranes in chloroplasts, state transitions, and, ultimately, the evolutionary success of plants.

In vitreous sections, the PSII arrays are confined to grana stacks. Arrays with the same lattice dimensions were also present in isolated membranes where two thylakoid vesicles were in contact through their stromal surfaces. In swollen thylakoid vesicles, ordered arrays were found only in such contact areas, whereas single membranes in the same vesicle showed no signs of order. This was also true of completely destacked grana membranes. It follows that the formation of regular PSII arrays in situ depends on the interaction of the stromal membrane surface across the 3.2-nm stromal gap, rather than on the interaction of the OECs across the lumenal gap, or on lateral contacts within the membrane.

However, interdigitating OECs could give rise to long-range order in the direction perpendicular to the membrane plane, such that several crystalline membrane pairs form one large, paracrystalline 3D array. Such larger-scale arrays might explain the long-standing, puzzling observation of a strong CD signal associated with stacked grana thylakoids (Barzda et al. 1994), indicative of 3D long-range order of chlorophyll-containing complexes. A similar strong CD signal is observed with crystalline aggregates of LHCII (Barzda et al., 1994), yet no such LHCII aggregates have ever been identified in grana stacks, and the PSII arrays were thought to form only under special circumstances. Our results now indicate that LHCII is in fact part of the crystalline PSII arrays and that these arrays do occur in normal high-light chloroplasts. The CD signal thus most likely reflects the long-range order of chlorophyll-protein complexes in the PSII supercomplex arrays.

The lateral segregation of chloroplast thylakoids into stroma and grana membranes and the tight appression of grana thylakoids are central characteristics of plant photosynthesis, yet its molecular basis has not been well understood until now. It is widely assumed that electrostatic interactions between LHCs are a major factor in grana formation and, hence, lateral segregation (Mullet and Arntzen, 1980; Allen, 1992; Standfuss et al.,

2005), but without a high-resolution structure of LHCII, this had to remain an assumption. The atomic structure suggested that LHCII trimers in grana thylakoids interact with one another by charge complementarity like molecular Velcro (Standfuss et al., 2005). Our membrane model (Figure 4) now indicates that this is indeed how LHCII trimers interact in grana stacks. Sequence comparison shows that the distribution of surface charges in CP26 and CP29 is likely to be similar to that in LHCII (Barros and Kühlbrandt, 2009). Interestingly, the densities in the PSII/LHCII supercomplex that have been ascribed to these minor LHCs are likewise on top of one another in our membrane model. Our model thus suggests that, in addition to LHCII, minor LHCs as well as PSII reaction centers themselves may contribute to stacking. This would explain the observation that grana stacking occurs also in the absence of LHCII (Andersson et al., 2003; Kim et al., 2009)

ATP Synthase and Membrane Curvature

The ATP synthase must be excluded from grana stacks for the simple reason that the stromal gap is too narrow to accommodate the bulky cF_1 head, which extends ~16 nm above the membrane surface (Miller and Staehelin, 1976). This is confirmed by our cryotomographic study. The exclusive presence of the ATP synthase in the nonstacked grana end membranes, stroma thylakoids, and the lamellae connecting them is consistent with current ideas of lateral heterogeneity in chloroplast membranes (Dekker and Boekema, 2005). We found that the ATP synthase is more or less evenly distributed over these flat membrane surfaces and that it is mostly present as a monomer. Any associations of two or more molecules are explained by stochastic contacts. Our tomographic volumes of spinach and pea thylakoids show no evidence of ATP synthase dimers, nor do our native gels of the functionally intact complex (Figures 5F and 5G). We conclude that the chloroplast ATP synthase of higher plants does not form oligomers in the membrane, in contrast with the mitochondrial ATP synthase (Strauss et al., 2008).

In mitochondria, ribbons of ATP synthase dimers are consistently found at the tightly curved edges of lamellar cristae or in narrow tubular cristae (Strauss et al., 2008). The difference in membrane curvature associated with the ATP synthase in chloroplasts or mitochondria may reflect the different electrochemical conditions in the two organelles. The lumenal pH in active chloroplasts is around 5, whereas the stromal pH is around 8, similar to that of the mitochondrial matrix. The pH difference (ΔpH) across the thylakoid membrane is thus up to 3 pH units, whereas the membrane poteintial $\Delta\Psi$ is small (Kaim and Dimroth, 1999; Kramer et al., 2003). By contrast, mitochondria are characterized by a comparatively high $\Delta\Psi$ and a small ΔpH of <1 pH unit between the intermembrane space and the matrix.

In vitro, ATP synthases (mitochondrial, chloroplast, or bacterial) require an external pH well below 6 for efficient ATP production (von Ballmoos et al., 2009). Evidently, the proton concentration at higher external pH is insufficient to drive ATP synthesis, even at a high membrane potential (von Ballmoos et al., 2009; Wiedenmann et al., 2009). Therefore, although $\Delta\Psi$ and ΔpH are thermodynamically equivalent, they are not kinetically equivalent; a high membrane potential cannot compensate fully for a lack of protons. It has been proposed that in mitochondria, the cristae of the inner membrane work as proton traps, funneling the protons pumped out of the matrix by the respiratory chain complexes to the ATP synthase dimers (Strauss et al., 2008). The high ΔpH across the thylakoid membrane means that this is not necessary in chloroplasts. A high local membrane curvature around the chloroplast ATP synthase would therefore not confer an evolutionary advantage. This hypothesis is fully consistent with the findings that the mitochondrial ATP synthase seems to be preferentially associated with regions of high membrane curvature (Strauss et al., 2008), whereas the opposite is true for the chloroplast ATP synthase (this work).

Conclusion

Tomographic volumes of vitreous thin sections and isolated thylakoid membranes have revealed the organization of PSII in thylakoid grana. We show that PSII in grana stacks is mostly, if not entirely, dimeric and that the dimeric PSII/LHCII supercomplexes form regular crystalline arrays in normal, high light–treated chloroplasts. We present a model that explains grana stacking through the interaction by charge complementarity of LHCII trimers and other chlorophyll-protein complexes across the 3.2-nm stromal gap. This interaction has clear implications for the size and efficiency of the photosynthetic antenna in plant chloroplasts.

We show that the chloroplast ATP synthase is monomeric and confined to flat or minimally curved regions of the thylakoid membrane, where it is distributed equally and randomly in high copy numbers of 1770 per μm^2. This is in stark contrast with the mitochondrial ATP synthase, which is preferentially, if not exclusively, arranged in long dimer rows along tightly curved membrane regions. There is an apparent link between ΔpH, external pH, and membrane curvature, such that the small ΔpH and comparatively high external pH in mitochondria requires special membrane compartments, the cristae, to capture protons for ATP synthesis. This is not the case in chloroplast thylakoids, where the large ΔpH and low lumenal pH in thylakoids ensures efficient ATP production without a highly curved membrane environment for the ATP synthase.

MATERIALS AND METHODS

Plant Materials and Growth Conditions

For chloroplast isolation, green house–grown spinach (*Spinacia oleracea*) and pea (*Pisum sativum*) plants were used. Alternatively, pea plants were grown in a growth chamber (10 h of light at 10.000 lx, 14 h of darkness) at 21°C and a relative humidity of 30%. To maximize the yield of material, chloroplasts were isolated when the leaves were fully developed (2 to 3 weeks after germination for pea and ~8 weeks after germination for spinach).

Thylakoid Membrane Preparation by Digitonin Solubilization

Thylakoid membranes were isolated from spinach leaves, following the standard MDT isolation procedure of Dunahay et al. (1984) in detail

without modification. Briefly, 100 g of spinach leaves were deveined and macerated in solution M-1 (250 mL of 0.4 M NaCl, 2 mM $MgCl_2$, 0.2% BSA, and 20 mM Tricine, pH 8.0) in a Waring blender. The slurry was filtered through four layers of cheesecloth, and centrifuged at 300*g* for 1 min to remove debris. The supernatant was centrifuged at 4000*g* for 10 min, and the pellet was washed once in solution M-2 (0.15 M NaCl, 5 mM $MgCl_2$, 0.2% BSA, and 20 mM Tricine, pH 8.0). The pellet was suspended in solution M-3 (330 mM sorbitol, 15 mM NaCl, 4 mM $MgCl_2$, and 10 mM MES, pH 6.5). The chlorophyll concentration was adjusted to 1.0 mg/mL, and an equal volume of 0.5% digitonin in M-3 solution was added, and the suspension was allowed to rest on ice for 5 min. This mixture was diluted 10-fold with M-3 and centrifuged at 10,000*g* for 30 min. The pellet was resuspended in solution M-3, the chlorophyll concentration was adjusted to 1.0 mg/mL, and an equal volume of 0.4% Triton X-100 in solution Y-3 (0.33 M sorbitol, 4 mM $MgCl_2$, and 10 mM MES, pH 6.5) was added. After 5 min on ice, the mixture was diluted 10-fold with solution M-3 and centrifuged at 12,000*g* for 30 min. The resulting pellet was resuspended in M-3 solution.

Thylakoid Membrane Preparation by Osmotic Shock

Thylakoids not exposed to any detergent were isolated by the standard protocol of Joy and Mills (1987) with minor modifications to improve purity. Briefly, 30 g of leaf material were blended in 180 mL 330 mM sorbitol, 50 mM Tricine, pH 7.5, 2 mM EDTA, 1 mM MgCl, and 0.1% (w/v) BSA. The suspension was filtered and then centrifuged for 7 min at 1000*g*. The pellet was resuspended in 330 mM sorbitol, 2 mM EDTA, 1 mM $MgCl_2$, 0.1% (w/v) BSA, and 50 mM Tricine, pH 7.5, before being applied to a 40%/80% Percoll step gradient in the same buffer without BSA. After centrifugation at 3200*g* for 15 min, the green band at the Percoll step was isolated and washed in 330 mM sorbitol, 2 mM EDTA, 1 mM $MgCl_2$ and 50 mM Tricine pH 7.5. A 3 μL sample of this chloroplast suspension was placed on a Quantifoil EM grid (200 mesh, R2/2; Quantifoil Micro Tools) and vitrified by plunge-freezing (see Supplemental Movie online). Thylakoids were extracted after breaking up chloroplasts by hypo-osmotic shock (10 mM NaCl, 2 mM EDTA, 1 mM $MgCl_2$, and 10 mM Tricine, pH 7.5). Thylakoid membranes were separated from soluble protein and debris by centrifugation at 3200*g* for 10 min and resuspended in the same buffer. Chloroplasts and membranes were continuously illuminated with fluorescent light at ~800 lx during all preparation steps.

Plunge-Freezing of Thylakoid Membranes in Solution

Isolated thylakoid membranes were vitrified by plunge-freezing (Dubochet et al., 1988) using Quantifoil EM grids (200 mesh, R2/2; Quantifoil Micro Tools) with holey carbon support film and a home-built guillotine plunge-freezer. As previously described (Nicastro et al., 2006), the grids were made hydrophilic by glow discharging. Optionally, 6- or 10-nm colloidal gold (Sigma-Aldrich) was applied and dried onto the grid for later use as fiducial markers for tilt series alignment. Two to four microliters of sample solution and 1 to 2 μL of 6- or 10-nm colloidal gold solution was applied to the grid, briefly mixed, and blotted from both sides with Whatman #1 filter paper. Immediately after blotting, the grid was plunge-frozen in liquid ethane cooled with liquid nitrogen. The vitrified grids were transferred into liquid nitrogen and stored until use.

Vitreous Sections of Intact Chloroplasts

Sections of frozen-hydrated chloroplasts were prepared as previously described (Ladinsky et al., 2006). Briefly, intact chloroplasts were isolated from spinach leaves using the MDT method (Dunahay et al., 1984) as described above, but without the detergent step. Whole chloroplasts in 330 mM sorbitol, 15 mM NaCl, 4 mM $MgCl_2$, and 10 mM MES, pH 6.5, were rapidly frozen using a HPM-010 high-pressure freezer (Bal-Tec). The chloroplast suspension was frozen inside two-piece brass planchettes. The domed half of the planchette was coated with lecithin prior to filling with sample for ease of separation of the two halves after freezing. After splitting the planchettes under liquid nitrogen, the vitrified sample remained in the flat half of the freezer hats, while dome-shaped side of the sample was exposed. Using an UltraCut-UCT microtome equipped with an EM-FCS cryostage (Leica Microsystems) and cryodiamond trimming tools or knives (Diatome), the dome was appropriately trimmed and then vitreous sections with an effective thickness of ~150 nm (as measured by the thickness of reconstructed tomograms) were cut at temperatures below the devitrification temperature of about −135°C. Vitreous sections were transferred and stamped onto carbon-coated 200-mesh molybdenum EM grids (Electron Microscopy Sciences). The grids with vitreous sections were stored in liquid nitrogen until inspection with the electron microscope.

EM

Tomograms were collected using either a TECNAI F30 or a FEI Polara electron microscope (FEI). Both microscopes were equipped with a field-emission gun operating at 300 keV, high-tilt stage, postcolumn energy filter, and sensitive 2k × 2k CCD camera (Gatan). Grids were loaded under liquid nitrogen into a high-tilt side entry cryoholder (Gatan 626) for the Tecnai F30 or in cartridges for the multispecimen carrier of the Polara. Uniaxial tilt series were recorded from +65° to −65° at intervals of 1 to 1.7°, using the microscope control program SerialEM (Mastronarde, 2005) or the FEI tomography software. The chosen magnification corresponded to 0.711-mm pixel size for the vitreous sections and 0.57- or 0.99-nm pixel size for the isolated thylakoids. The total dose used was 1 to 1.5 × 10^4 e/nm^2. All tomograms were recorded with zero loss filtering (slit width 20 eV) at a defocus of −6 to −10 μm.

Image Processing

Tomograms were generated from the raw image stacks using the IMOD software package (Kremer et al., 1996). The tilt series images were either aligned using gold fiducials (isolated thylakoids) (Mastronarde, 2006) or fiducial-less cross-correlation alignment (vitreous chloroplast sections), then reconstructed into tomograms and analyzed. Signal-to-noise ratio of the ATP synthase and the PSII supercomplexes was increased by subtomogram averaging using the IMOD (Kremer et al., 1996) and Particle Estimation for Electron Tomography software (Nicastro et al., 2006), as previously described (Nicastro et al., 2006). Subtomograms containing similar particles were extracted from the tomograms, aligned using 3D cross-correlation, and averaged with appropriate weighting to correct for the missing wedge. For averages of the ATP synthase, the PSII complex and the crystalline array of supercomplexes, 50, 313, or 100 particles were used, respectively. The periodicity of grana stacks or PSII arrays was determined from the power spectra of slices through a tomographic volume, cut either in the direction perpendicular to the membrane plane (for grana stacks) or along the membrane plane (for PSII arrays). The power spectrum of an object is the square of its Fourier transform. Power spectra are calculated routinely in image processing for convenient, reliable, and accurate analysis of periodic structures. Manual segmentation and automated isosurface rendering of the tomographic volumes was performed with AMIRA (Mercury Systems). The structure of the PSII/LHCII supercomplex (Nield and Barber, 2006) was filtered to 3-nm resolution using the EMAN software (NCMI) and fitted into the averaged PSII lattice using Chimera Software (University of San Francisco, CA).

Clear-Native PAGE

Native gel electrophoresis and in-gel staining for ATPase activity of oligomers was performed according to Wittig and Schägger (2005).

Briefly, isolated chloroplasts at a chlorophyll concentration of 2 mg/mL were solubilized with 1 to 3% digitonin. Insoluble material was pelleted at 13,000*g* for 10 min, and the supernatant was separated on a native 3 to 10% acrylamide gel at 150 V for 6 h at 4°C. The gel was incubated in assay buffer (270 mM glycine, 16 mM $MgCl_2$, 8 mM ATP, 0.2% lead nitrate, and 35 mM Tris, pH 8.4) for 5 h. ATPase activity was detected by the appearance of a white precipitate of lead phosphate. To analyze the subunit composition of the native gel bands, second-dimension denaturing PAGE was performed. Briefly, a strip from the clear-native gel was soaked for 1 h in 25 mM Tris, 192 mM Glycin, and 0.1% SDS and subsequently inserted into a 4% stacking gel of a freshly cast 15% Tris SDS-PAGE. As running buffer, 25 mM Tris, 192 mM Glycin, and 0.1% SDS was used. After running, the gel bands were stained with Coomassie Brilliant Blue according to Studier (2005).

Supplemental Data

The following material is available in the online version of this article.

Supplemental Movie. Tomographic Volume of Part of a Whole Pea Chloroplast, Ruptured by Blotting on the EM Grid Seconds before Plunge-Freezing in Liquid Ethane.

ACKNOWLEDGMENTS

We thank John Nield for providing the model of the PSII/LHCII supercomplex and Karen Davies, Bastian Barton, and Götz Hofhaus for scientific advice. We thank Mike Strauss for suggestions and help concerning electron tomography, Enrico Schleiff and members of his group for help with pea chloroplast isolation, Mark Ladinsky for cutting vitreous sections, and Remco Wouts and Reinhardt Maas for computer assistance. Much of this work would not have been possible without Deryck Mills, who keeps the Frankfurt EM facility in perfect shape. The work was supported in part by RR000592 from the National Institutes of Health to D.N. and J.R.M.

Received September 16, 2009; revised March 3, 2010; accepted March 29, 2010; published April 13, 2010.

REFERENCES

Al-Amoudi, A., Studer, D., and Dubochet, J. (2005). Cutting artefacts and cutting process in vitreous sections for cryo-electron microscopy. J. Struct. Biol. **150:** 109–121.

Albertsson, P.-A. (1982). Interaction between the lumenal sides of the thylakoid membrane. FEBS Lett. **149:** 186–190.

Allen, J.F. (1992). Protein phosphorylation in regulation of photosynthesis. Biochim. Biophys. Acta **1098:** 275–335.

Anderson, J.M., Chow, W.S., and De Las Rivas, J. (2008). Dynamic flexibility in the structure and function of photosystem II in higher plant thylakoid membranes: the grana enigma. Photosynth. Res. **98:** 575–587.

Andersson, B., and Anderson, J.M. (1980). Lateral heterogeneity in the distribution of chlorophyll-protein complexes of the thylakoid membranes of spinach chloroplasts. Biochim. Biophys. Acta **593:** 427–440.

Andersson, J., Wentworth, M., Walters, R.G., Howard, C.A., Ruban, A. V., Horton, P., and Jansson, S. (2003). Absence of the Lhcb1 and Lhcb2 proteins of the light-harvesting complex of photosystem II - Effects on photosynthesis, grana stacking and fitness. Plant J. **35:** 350–361.

Armond, P.A., Staehelin, L.A., and Arntzen, C.J. (1977). Spatial relationship of photosystem I, photosystem II, and the light-harvesting complex in chloroplast membranes. J. Cell Biol. **73:** 400–418.

Arvidsson, P.-O., and Sundby, C. (1999). A model for the topology of the chloroplast thylakoid membrane. Aust. J. Plant Physiol. **26:** 687–694.

Austin, J.R., 2nd, Frost, E., Vidi, P.A., Kessler, F., and Staehelin, L.A. (2006). Plastoglobules are lipoprotein subcompartments of the chloroplast that are permanently coupled to thylakoid membranes and contain biosynthetic enzymes. Plant Cell. **18:** 1693–1703.

Baniulis, D., Yamashita, E., Zhang, H., Hasan, S.S., and Cramer, W.A. (2008). Structure-function of the cytochrome b6f complex. Photochem. Photobiol. **84:** 1349–1358.

Barbato, R., Friso, G., Rigoni, F., Dalla Vecchia, F., and Giacometti, G.M. (1992). Structural changes and lateral redistribution of photosystem II during donor side photoinhibition of thylakoids. J. Cell Biol. **119:** 325–335.

Barber, J. (1982). Influence of surface-charges on thylakoid structure and function. Annu. Rev. Plant Physiol. Plant Mol. Biol. **33:** 261–295.

Barros, T., and Kühlbrandt, W. (2009). Crystallisation, structure and function of plant light-harvesting complex II. Biochim. Biophys. Acta **1787:** 753–772.

Barzda, V., Mustárdy, L., and Garab, G. (1994). Size dependency of circular dichroism in macroaggregates of photosynthetic pigment-protein complexes. Biochemistry **33:** 10837–10841.

Betterle, N., Ballottari, M., Zorzan, S., de Bianchi, S., Cazzaniga, S., Dall'osto, L., Morosinotto, T., and Bassi, R. (2009). Light-induced dissociation of an antenna hetero-oligomer is needed for non-photochemical quenching induction. J. Biol. Chem. **284:** 15255–15266.

Boekema, E.J., Hankamer, B., Bald, D., Kruip, J., Nield, J., Boonstra, A.F., Barber, J., and Rogner, M. (1995). Supramolecular structure of the photosystem II complex from green plants and cyanobacteria. Proc. Natl. Acad. Sci. USA **92:** 175–179.

Boekema, E.J., Nield, J., Hankamer, B., and Barber, J. (1998). Localization of the 23-kDa subunit of the oxygen-evolving complex of photosystem II by electron microscopy. Eur. J. Biochem. **252:** 268–276.

Boekema, E.J., van Breemen, J.F., van Roon, H., and Dekker, J.P. (2000). Arrangement of photosystem II supercomplexes in crystalline macrodomains within the thylakoid membrane of green plant chloroplasts. J. Mol. Biol. **301:** 1123–1133.

Boekema, E.J., Van Roon, H., Van Breemen, J.F., and Dekker, J.P. (1999). Supramolecular organization of photosystem II and its light-harvesting antenna in partially solubilized photosystem II membranes. Eur. J. Biochem. **266:** 444–452.

Böttcher, B., and Graber, P. (2000). The structure of the H(+)-ATP synthase from chloroplasts and its subcomplexes as revealed by electron microscopy. Biochim. Biophys. Acta **1458:** 404–416.

Dekker, J.P., and Boekema, E.J. (2005). Supramolecular organization of thylakoid membrane proteins in green plants. Biochim. Biophys. Acta **1706:** 12–39.

Dubochet, J., Adrian, M., Chang, J.J., Homo, J.C., Lepault, J., McDowall, A.W., and Schultz, P. (1988). Cryo-electron microscopy of vitrified specimens. Q. Rev. Biophys. **21:** 129–228.

Dunahay, T.G., Staehelin, L.A., Seibert, M., Ogilvie, P.D., and Berg, S.P. (1984). Structural, biochemical and biophysical characterization of four oxigen-evolving photosystem II preparations from spinach. Biochim. Biophys. Acta **764:** 179–193.

Ferreira, K.N., Iverson, T.M., Maghlaoui, K., Barber, J., and Iwata, S. (2004). Architecture of the photosynthetic oxygen-evolving center. Science **303:** 1831–1838.

Frey, T.G., and Mannella, C.A. (2000). The internal structure of mitochondria. Trends Biochem. Sci. **25:** 319–324.

Fromme, P., and Grotjohann, I. (2008). Structure of Photosystems I and II. Results Probl. Cell Differ. **45:** 33–72.

Garber, M.P., and Steponkus, P.L. (1976). Alterations in chloroplast thylakoids during cold acclimation. Plant Physiol. **57:** 681–686.

Hankamer, B., Morris, E.P., and Barber, J. (1999). Revealing the structure of the oxygen-evolving core dimer of photosystem II by cryoelectron crystallography. Nat. Struct. Biol. **6:** 560–564.

Hankamer, B., Nield, J., Zheleva, D., Boekema, E., Jansson, S., and Barber, J. (1997). Isolation and biochemical characterisation of monomeric and dimeric photosystem II complexes from spinach and their relevance to the organisation of photosystem II in vivo. Eur. J. Biochem. **243:** 422–429.

Jansson, S., Stefansson, H., Nyström, U., Gustafsson, P., and Albertsson, P.-Å. (1997). Antenna protein composition of PS I and PS II in thylakoid sub-domains. Biochim. Biophys. Acta **1320:** 297–309.

Jensen, P.E., Bassi, R., Boekema, E.J., Dekker, J.P., Jansson, S., Leister, D., Robinson, C., and Scheller, H.V. (2007). Structure, function and regulation of plant photosystem I. Biochim. Biophys. Acta **1767:** 335–352.

Joy, K.W., and Mills, W.R. (1987). Purification of chloroplasts using silica sols. Methods Enzymol. **148:** 179–188.

Kaim, G., and Dimroth, P. (1999). ATP synthesis by F-type ATP synthase is obligatorily dependent on the transmembrane voltage. EMBO J. **18:** 4118–4127.

Kern, J., and Renger, G. (2007). Photosystem II: Structure and mechanism of the water:plastoquinone oxidoreductase. Photosynth. Res. **94:** 183–202.

Kim, E.H., Li, X.P., Razeghifard, R., Anderson, J.M., Niyogi, K.K., Pogson, B.J., and Chow, W.S. (2009). The multiple roles of light-harvesting chlorophyll a/b-protein complexes define structure and optimize function of Arabidopsis chloroplasts: A study using two chlorophyll b-less mutants. Biochim. Biophys. Acta **1787:** 973–984.

Kirchhoff, H., Haase, W., Wegner, S., Danielsson, R., Ackermann, R., and Albertsson, P.A. (2007). Low-light-induced formation of semi-crystalline photosystem II arrays in higher plant chloroplasts. Biochemistry **46:** 11169–11176.

Kirchhoff, H., Lenhert, S., Buchel, C., Chi, L., and Nield, J. (2008). Probing the organization of photosystem II in photosynthetic membranes by atomic force microscopy. Biochemistry **47:** 431–440.

Kramer, D.M., Cruz, J.A., and Kanazawa, A. (2003). Balancing the central roles of the thylakoid proton gradient. Trends Plant Sci. **8:** 27–32.

Kremer, J.R., Mastronarde, D.N., and McIntosh, J.R. (1996). Computer visualization of three-dimensional image data using IMOD. J. Struct. Biol. **116:** 71–76.

Kreuz, K., Dehesh, K., and Apel, K. (1986). The light-dependent accumulation of the P700 chlorophyll a protein of the photosystem I reaction center in barley. Evidence for translational control. Eur. J. Biochem. **159:** 459–467.

Kruse, O., Zheleva, D., and Barber, J. (1997). Stabilization of photosystem two dimers by phosphorylation: implication for the regulation of the turnover of D1 protein. FEBS Lett. **408:** 276–280.

Kühlbrandt, W. (1987). Three-dimensional crystals of the light-harvesting chlorophyll a/b protein complex from pea chloroplasts. J. Mol. Biol. **194:** 757–762.

Ladinsky, M.S., Pierson, J.M., and McIntosh, J.R. (2006). Vitreous cryo-sectioning of cells facilitated by a micromanipulator. J. Microsc. **224:** 129–134.

Leis, A., Rockel, B., Andrees, L., and Baumeister, W. (2009). Visualizing cells at the nanoscale. Trends Biochem. Sci. **34:** 60–70.

Machold, O., Simpson, D.J., and Høyer-Hansen, G. (1977). Correlation between the freeze fracture appearance and polypeptide composition of thylakoid membranes in barley. Carlsberg Res. Commun. **42:** 499–516.

Mannella, C.A. (2001). Application of electron tomography to mitochondrial research. Methods Cell Biol. **65:** 245–256.

Mastronarde, D.N. (2005). Automated electron microscope tomography using robust prediction of specimen movements. J. Struct. Biol. **152:** 36–51.

Mastronarde, D.N. (2006). Fiducial marker and hybrid alignment methods for single- and double-axis tomography. In Electron Tomography: Methods for Three-Dimensional Visualization of Structures in the Cell, J. Frank, ed (Berlin: Springer), pp. 163–185.

Mellwig, C., and Böttcher, B. (2003). A unique resting position of the ATP-synthase from chloroplasts. J. Biol. Chem. **278:** 18544–18549.

Miller, K.R., Bloodgood, R.A., and Staehelin, L.A. (1976). Crystals within thylakoids: a structural analysis. J. Ultrastruct. Res. **54:** 29–36.

Miller, K.R., and Staehelin, L.A. (1976). Analysis of the thylakoid outer surface. Coupling factor is limited to unstacked membrane regions. J. Cell Biol. **68:** 30–47.

Morosinotto, T., Bassi, R., Frigerio, S., Finazzi, G., Morris, E., and Barber, J. (2006). Biochemical and structural analyses of a higher plant photosystem II supercomplex of a photosystem I-less mutant of barley. Consequences of a chronic over-reduction of the plastoquinone pool. FEBS J. **273:** 4616–4630.

Morris, E.P., Hankamer, B., Zheleva, D., Friso, G., and Barber, J. (1997). The three-dimensional structure of a photosystem II core complex determined by electron crystallography. Structure **5:** 837–849.

Mullet, J.E., and Arntzen, C.J. (1980). Simulation of grana stacking in a model membrane system. Mediation by a purified light-harvesting pigment-protein complex from chloroplasts. Biochim. Biophys. Acta **589:** 100–117.

Murakami, S., and Packer, L. (1970). Light-induced changes in the conformation and configuration of the thylakoid membrane of Ulva and Porphyra chloroplasts in vivo. Plant Physiol. **45:** 289–299.

Mustardy, L., Buttle, K., Steinbach, G., and Garab, G. (2008). The three-dimensional network of the thylakoid membranes in plants: quasihelical model of the granum-stroma assembly. Plant Cell **20:** 2552–2557.

Mustardy, L., and Garab, G. (2003). Granum revisited. A three-dimensional model–where things fall into place. Trends Plant Sci. **8:** 117–122.

Neff, D., and Dencher, N.A. (1999). Purification of multisubunit membrane protein complexes: Isolation of chloroplast FoF_1- ATP-synthase, CF_o and CF_1 by blue native electrophoresis. Biochem. Biolphys. Res. Commun. **259:** 569–575.

Nelson, N., and Ben-Shem, A. (2004). The complex architecture of oxygenic photosynthesis. Nat. Rev. Mol. Cell Biol. **5:** 971–982.

Nicastro, D., Frangakis, A.S., Typke, D., and Baumeister, W. (2000). Cryo-electron tomography of neurospora mitochondria. J. Struct. Biol. **129:** 48–56.

Nicastro, D., Schwartz, C., Pierson, J., Gaudette, R., Porter, M.E., and McIntosh, J.R. (2006). The molecular architecture of axonemes revealed by cryoelectron tomography. Science **313:** 944–948.

Nield, J., and Barber, J. (2006). Refinement of the structural model for the photosystem II supercomplex of higher plants. Biochim. Biophys. Acta **1757:** 353–361.

Nield, J., Orlova, E.V., Morris, E.P., Gowen, B., van Heel, M., and Barber, J. (2000). 3D map of the plant photosystem II supercomplex obtained by cryoelectron microscopy and single particle analysis. Nat. Struct. Biol. **7:** 44–47.

Nir, I., and Pease, D.C. (1973). Chloroplast organization and the ultrastructural localization of photosystems I and II. J. Ultrastruct. Res. **42:** 534–550.

Oleszko, S., and Moudrianakis, E.N. (1974). The visualization of the photosynthetic coupling factor in embedded spinach chloroplasts. J. Cell Biol. **63:** 936–948.

Park, R.B. (1965). Substructure of chloroplast lamellae. J. Cell Biol. **27:** 151–161.

Peter, G., and Thomber, J. (1991). Biochemical evidence that the

higher plant photosystem II core complex is organized as a dimer. Plant Cell Physiol. **32:** 1237–1250.

Renger, G., and Renger, T. (2008). Photosystem II: The machinery of photosynthetic water splitting. Photosynth. Res. **98:** 53–80.

Rexroth, S., Meyer Zu Tittingdorf, J.M., Schwassmann, H.J., Krause, F., Seelert, H., and Dencher, N.A. (2004). Dimeric H^+-ATP synthase in the chloroplast of *Chlamydomonas reinhardtii*. Biochim. Biophys. Acta **1658:** 202–211.

Santini, C., Tidu, V., Tognon, G., Ghiretti Magaldi, A., and Bassi, R. (1994). Three-dimensional structure of the higher-plant photosystem II reaction centre and evidence for its dimeric organization in vivo. Eur. J. Biochem. **221:** 307–315.

Schmid, V.H. (2008). Light-harvesting complexes of vascular plants. Cell Mol. Life Sci. **65:** 3619–3639.

Seibert, M., DeWit, M., and Staehelin, L.A. (1987). Structural localization of the O_2-evolving apparatus to multimeric (tetrameric) particles on the lumenal surface of freeze-etched photosynthetic membranes. J. Cell Biol. **105:** 2257–2265.

Shimoni, E., Rav-Hon, O., Ohad, I., Brumfeld, V., and Reich, Z. (2005). Three-dimensional organization of higher-plant chloroplast thylakoid membranes revealed by electron tomography. Plant Cell **17:** 2580–2586.

Simpson, D.J. (1983). Freeze-fracture studies on barley plastid membranes. VI. Location of the P700-chlorophyll a-protein 1. Eur. J. Cell Biol. **31:** 305–314.

Staehelin, L.A. (1975). Chloroplast membrane structure. Intramembranous particles of different sizes make contact in stacked membrane regions. Biochim. Biophys. Acta **408:** 1–11.

Staehelin, L.A. (1986). Chloroplast structure and supramolecular organization of photosynthetic membranes. **Encyc. Plant Physiol. 19:** 1–84.

Staehelin, L.A., Armond, P.A., and Miller, K.R. (1976). Chloroplast membrane organization at the supramolecular level and its functional implications. Brookhaven Symp. Biol. **28:** 278–315.

Standfuss, J., Terwisscha van Scheltinga, A.C., Lamborghini, M., and Kühlbrandt, W. (2005). Mechanisms of photoprotection and nonphotochemical quenching in pea light-harvesting complex at 2.5 A resolution. EMBO J. **24:** 919–928.

Stock, D., Leslie, A.G., and Walker, J.E. (1999). Molecular architecture of the rotary motor in ATP synthase. Science **286:** 1700–1705.

Strauss, M., Hofhaus, G., Schröder, R.R., and Kühlbrandt, W. (2008). Dimer ribbons of ATP synthase shape the inner mitochondrial membrane. EMBO J. **27:** 1154–1160.

Studier, F.W. (2005). Protein production by auto-induction in high density shaking cultures. Protein Expr. Purif. **41:** 207–234.

Tokuyasu, K.T. (1976). Membranes as observed in frozen sections. J. Ultrastruct. Res. **55:** 281–287.

van Roon, H., van Breemen, J.F., de Weerd, F.L., Dekker, J.P., and Boekema, E.J. (2000). Solubilization of green plant thylakoid membranes with n-dodecyl-alpha,D-maltoside. Implications for the structural organization of the photosystem II, photosystem I, ATP synthase and cytochrome b6 f complexes. Photosynth. Res. **64:** 155–166.

von Ballmoos, C., Wiedenmann, A., and Dimroth, P. (2009). Essentials for ATP synthesis by F1F0 ATP synthases. Annu. Rev. Biochem. **78:** 649–672.

Watanabe, M., Iwai, M., Narikawa, R., and Ikeuchi, M. (2009). Is the photosystem II complex a monomer or a dimer? Plant Cell Physiol. **50:** 1674–1680.

Wehrmeyer, W. (1964). Über Membranbildungsprozesse in Chloroplasten. II. Zur Entstehung der Grana durch Membranüberschiebung. Planta **63:** 10–30.

Wiedenmann, A., Dimroth, P., and von Ballmoos, C. (2009). Functional asymmetry of the F(0) motor in bacterial ATP synthases. Mol. Microbiol. **72:** 479–490.

Wittig, I., and Schägger, H. (2005). Advantages and limitations of clear-native PAGE. Proteomics **5:** 4338–4346.

Arrangement of Photosystem II and ATP Synthase in Chloroplast Membranes of Spinach and Pea

Bertram Daum, Daniela Nicastro, Jotham Austin, II, J. Richard McIntosh and Werner Kühlbrandt

PLANT CELL published online Apr 13, 2010;
DOI: 10.1105/tpc.109.071431